Droplet Formation, Detachment, and Impingement on the Molten Pool in Gas Metal Arc Welding

H.G. FAN and R. KOVACEVIC

A mathematical model is developed to describe the globular transfer in gas metal arc welding (GMAW). This work is both theoretical and experimental. Using the volume-of-fluid (VOF) method, the fluid-flow and heat-transfer phenomena are dynamically studied during the following processes: droplet formation and detachment, impingement of a droplet on a solid substrate, impingement of multiple droplets on the molten pool, and solidification after the arc extinguishes. A He-Ne laser, in conjunction with the shadow graphing technique, is used to observe the metal transfer processes. Theoretical predictions and experimental results are in close agreement, suggesting that the theoretical treatment of the model is good.

I. INTRODUCTION

GAS metal arc welding (GMAW) is an arc welding process that uses an arc between a continuous, consumable filler-metal electrode and the weld pool (Figure 1). The GMAW process, due to its high productivity, has been the predominant welding process. Studying the transport phenomena in stationary GMAW could provide insight into what occurs in the processes of droplet formation, detachment, and impingement on the molten pool.

Two major models developed to describe the droplet formation are the static-force balance theory (SFBT)[1,2] and the magnetic pinch instability theory (PIT).[2,3,4] The SFBT considers the balance between gravity, electromagnetic forces, plasma drag force, and surface tension acting on a pendant drop. The PIT considers perturbation due to the magnetic pinch force acting on an infinite cylindrical column of liquid metal. Nemchinsky[5] developed a steady-state model to describe the equilibrium shape of a pendant droplet, accounting for surface tension and magnetic pinch force. A simple approximation for the current-density distribution in the droplet was used. Simpson and Zhu[6] developed a one-dimensional model which considered the forces acting on the droplet. The model makes the first predictions of droplet shape as a function of time. Recently, Haidar and Lowke[7] and Haidar[8] developed a time-dependent two-dimensional model for the prediction of droplet formation which includes the arc. The surface tension, gravity, and magnetic pinch forces were considered. However, the model did not consider the arc drag force, droplet detachment, and the impingement of the droplets on the molten pool.

The literature shows several images of globular transfer in GMAW.[9,10,11] Reference 12 shows a set of particularly well-specified, clear images of the transition from globular to rotating transfer. This collection of images is of moving, bead-on-plate GMAW. There is no attention paid to the impact effect of the droplet on the molten pool. The present experiment records the images of stationary GMAW to show that effect on the molten pool. Weld pool oscillation has been studied, and the information has been used in automatic control in gas tungsten arc welding;[13–16] but not so yet for GMAW, at least not specifically related to that oscillation which is triggered by the impingement of droplets as they fall into the weld pool.

The GMAW molten pool is less studied in theoretical aspects due to the interaction between the droplet and base metal. The impingement of molten metal droplets into the weld pool in GMAW affects the shape of the free surface and the convective heat transfer in the weld pool. Tsao and Wu[17] presented a two-dimensional stationary weld-pool convection model for GMAW which assumed the weld-pool surface to be flat and took into account the thermal energy exchange between the metal droplets and weld pool. Using boundary-fitted coordinates, Kim and Na[18] presented a three-dimensional quasi-steady model for the moving bead-on-plate GMAW process. The size and profile of the weld pool were predicted, but the dynamic interaction between the droplet and the weld pool free surface was not considered. Ushio and Wu[19] approximated the effect of the droplets on the weld pool as a constant force acting on the weld pool free surface, although the impingement process is not a continuous process. Recently, Choi *et al.*[20] used the volume of fluid (VOF) method to simulate the short-circuit mode metal transfer in stationary GMAW welding. However, the work did not include a description of thermal phenomena, rather, it assumed that the droplets and molten pool were isothermal. Adopting the VOF method, Trapaga[21] simulated fluid flow, heat transfer, and solidification of a single molten droplet impinging on a substrate in plasma spraying. But the multiple droplets in GMAW produce much-more-complex phenomena, including electromagnetic forces and Marangoni flow.

The formation of the metal droplets is governed by a combination of factors, including the balance of forces acting on the droplet, thermal phenomena in the wire, heat transfer from the arc, and the current density distribution in the droplet. It is clear that filler-metal droplets have an important influence on the weld pool in GMAW, since the droplets bring not only the impinging momentum but also a significant amount of thermal energy to the weld pool. So far, no mathematical model has been published for GMAW which combines the droplet formation and detachment and the dynamic interaction between the droplets and molten pool.

H.G. FAN, Research Associate, and R. KOVACEVIC, Professor, are with the Department of Mechanical Engineering, Southern Methodist University, Dallas, TX 75275.

Manuscript submitted October 20, 1998.

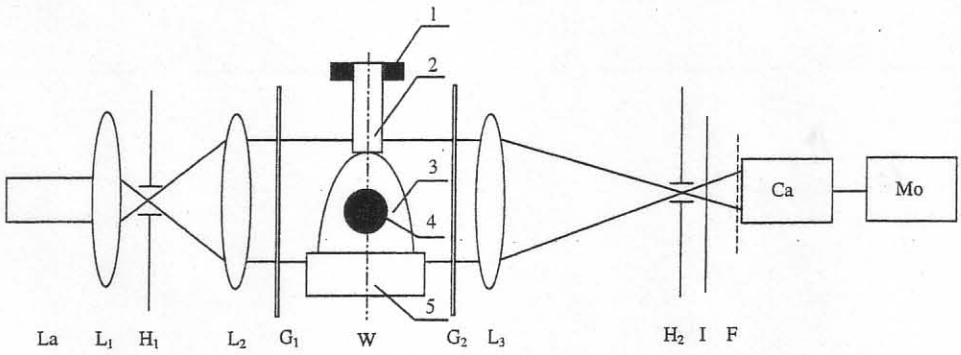

Fig. 1—Schematic diagram of photographic arrangement. La—laser; L_1, L_2, L_3—lenses; H_1, H_2—pin hole; G_1, G_2—protective transparent screen glasses; I—image screen; F—filter; Ca—camera; Mo—monitor; W—welding system (1, contact tube; 2, consumable electrode; 3, arc column; 4, droplet; 5, workpiece).

In this article, a new transient two-dimensional model is developed to simulate the droplet formation, detachment, and transport phenomena associated with a weld pool into which molten droplets periodically are injected. The formation and detachment of a droplet is driven by surface tension, arc drag force, gravity, and electromagnetic force. The solution algorithm–volume of fluid (SOLA–VOF)[22], modified to include heat transfer and the electromagnetic force, was used to track the transient shape of the droplet and the weld-pool surface. In addition, high-speed videography is used to record the welding process. The theoretical and experimental results are found to be in good agreement.

II. EXPERIMENTAL PROCEDURES

In GMAW, the various modes of metal transfer are classified into three main groups: free-flight transfer, bridging transfer, and slag-protected transfer.[2] In free-flight transfer, including globular, spray, and explosive transfer, the electrode does not contact the molten pool. Lesnewich[9] showed that the mode of metal transfer depends on many operational variables, such as welding current, electrode extension, electrode diameter, and polarity. Among these variables, welding current is the most common variable that is adjusted to obtain the desired metal transfer mode. At low welding currents, globular transfer occurs, while spray transfer occurs at relatively higher welding currents.

In the experiment, analysis of metal transfer was performed using high-speed videography with a laser-backlighted shadowgraphic method.[11] The setup of laser optics and the high-speed camera system is shown in Figure 1. A He-Ne laser was used as a background light source to exclude the high-intensity arc light. With the collimated light directed at the arc, a shadow graph of the droplet and molten pool was obtained. The high-speed video camera is capable of grabbing images at a maximum speed of 1000 full-frame pictures per second.

A power supply set in the constant-current mode was used to make stationary spot welds on a 4.8-mm-thick mild steel plate. The welding was performed under direct current, electrode-positive condition. The electrode used in this experiment was a mild steel welding wire with a diameter of 1.2 mm. The shielding gas used was pure argon. The electrode extension length between the contact tube and the tip of the electrode was 16 mm. Other experimental conditions are given in Table I. The droplet's size (D_d) was measured from the still image on the screen and averaged.

Table I. Welding Parameters, Some Determined by Measurements on High-Speed Films

Welding current I 160 A	Arc voltage U 29 V
Wire feed rate V_w 3.6 m/min	Droplet diameter D_d 3.1 mm
Droplet transfer frequency f	5 drops/s

Table II. Physical Properties of the Workpiece

Symbol	Value	Symbol	Value
β	10^{-4} K^{-1}	ρ	7200 kg/m^3
γ	1.2 N/m	μ_0	1.26×10^{-6} H/m
μ	0.006 kg/m · s	σ	7.7×10^5 mho/m
$d\gamma/dT$	10^{-4} N/m · K	ε	0.9
C_P	753 J/kg · K	ΔH	2.47×10^5 J/kg
T_l	1723 K	T_s	1523 K
k	20 W/m · K	K_{max}	10^4 s^{-1}

III. MATHEMATICAL FORMULATION

A. *Governing Equations*

In order to simplify the mathematical model, the following assumptions have been made:

(1) the welding process is assumed to be axisymmetric;
(2) laminar flow is assumed, since the size of the droplet and molten pool are small;
(3) the thermophysical properties listed in Table II are assumed constant;
(4) the fluid in the pool is driven by a combination of buoyancy, electromagnetic, and surface tension forces; and
(5) the heating effect of plasma on the traveling droplet is neglected.

Based on the previous assumptions, the governing differential equations used to describe heat and fluid flow in the electrode and weld pool can be expressed as follows.

Equation of mass continuity:

$$\frac{1}{r}\frac{\partial(ru)}{\partial r}+\frac{\partial w}{\partial z}=0 \qquad [1]$$

Conservation of radial momentum:

$$\frac{\partial}{\partial t}(\rho u)+\frac{1}{r}\frac{\partial}{\partial r}\left(\rho ruu-\mu r\frac{\partial u}{\partial r}\right)+\frac{\partial}{\partial z}\left(\rho uw-\mu\frac{\partial u}{\partial z}\right) \qquad [2]$$
$$=-\frac{\partial P}{\partial r}+\frac{1}{r}\frac{\partial}{\partial r}\left(\mu r\frac{\partial u}{\partial r}\right)-2\mu\frac{u}{r^2}+\frac{\partial}{\partial z}\left(\mu\frac{\partial w}{\partial r}\right)-j_z B_\theta-Ku$$

Conservation of axial momentum:

$$\frac{\partial}{\partial t}(\rho w)+\frac{1}{r}\frac{\partial}{\partial r}\left(\rho ruw-\mu r\frac{\partial w}{\partial r}\right)+\frac{\partial}{\partial z}\left(\rho ww-\mu\frac{\partial w}{\partial z}\right) \qquad [3]$$
$$=-\frac{\partial P}{\partial z}+\frac{1}{r}\frac{\partial}{\partial r}\left(\mu r\frac{\partial u}{\partial z}\right)+\frac{\partial}{\partial z}\left(\mu\frac{\partial w}{\partial z}\right)-Kw+S_w$$

$$S_w^{\text{pool}}=j_r B_\theta+\rho g\beta(T-T_r) \qquad [4]$$

$$S_w^{\text{electrode}}=j_r B_\theta-\rho g-\frac{3}{8}C_d\frac{V_{\text{arc}}^2\rho_{\text{arc}}}{R_d} \qquad [5]$$

The temperature-dependent drag term, which represents fluid flow in the mushy zone, is incorporated into the momentum equation *via Ku* and *Kw*, where

$$K=\begin{cases}0 & T>T_l\\ K_{\max}(T_l-T)/(T_l-T_s) & T_l\le T\le T_l\\ \infty & T<T_s\end{cases} \qquad [6]$$

The right-hand side of Eq. [5] represents the electromagnetic, gravity, and arc drag forces acting on the droplet. Here, C_d is the drag coefficient, V_{arc} is the velocity of the arc plasma, and ρ_{arc} is the density of the arc plasma. The calculation of arc drag force is detailed in Reference 2.

Conservation of energy:

$$\frac{\partial}{\partial t}(\rho h)+\frac{1}{r}\frac{\partial}{\partial r}\left(\rho ruh-r\frac{k}{C_p}\frac{\partial h}{\partial r}\right)+\frac{\partial}{\partial z}\left(\rho wh-\frac{k}{C_p}\frac{\partial h}{\partial z}\right) \qquad [7]$$
$$=\frac{j_r^2+j_z^2}{\sigma}-\Delta H\frac{\partial f_L}{\partial t}$$

In the energy equation, Ohmic heating is considered. Latent heat of fusion is included by employing the liquid fraction (f_L), which is defined as follows:

$$f_l=\begin{cases}1 & T>T_l\\ (T-T_s)/(T_l-T_s) & T_s\le T\le T_l\\ 0 & T<T_s\end{cases} \qquad [8]$$

where T_l and T_s are the liquidus and solidus temperatures, respectively.

Conservation of electrical charge:

In order to obtain the electromagnetic-force terms in Eqs. [2] and [3], the electric potential (ϕ) is calculated by solving the equation for current continuity,

$$\frac{1}{r}\frac{\partial}{\partial r}\left(\sigma r\frac{\partial\phi}{\partial r}\right)+\frac{\partial}{\partial z}\left(\sigma\frac{\partial\phi}{\partial z}\right)=0 \qquad [9]$$

and the current density is calculated from Ohm's law,

$$j_r=-\sigma\frac{\partial\phi}{\partial r}\qquad j_z=-\sigma\frac{\partial\phi}{\partial z} \qquad [10]$$

while the self-induced azimuthal magnetic field (B_θ) is derived from Ampere's law,

$$B_\theta=\frac{\mu_0}{r}\int_0^r j_z r dr \qquad [11]$$

No experimental measurements of the current density on a GMAW drop surface are available in the literature due to the difficulty of making such measurements in the harsh environment of the arc next to the free surface of a drop. Since it is difficult to determine the boundary condition, an approximation[5] is used to get the current-density distribution in the droplet. Let us assume that the axial current density is distributed uniformly over any horizontal cross section of the droplet:

$$j_z=\frac{I(z)}{2\pi R_d^2} \qquad [12]$$

where $I(z)$ is the current flowing through the droplet at distance of z from its tip. In our calculations, we used the linear approximation,[5] *i.e.*, $I(z)=I\cdot z/H$, where I is the total welding current, and H is the droplet length.

From Eq. [12] and the current-continuity Eq. [9], the radial current density in the droplet is

$$j_r=-\frac{r}{2}\frac{d}{dz}\left(\frac{I(z)}{\pi R_d^2}\right) \qquad [13]$$

and the magnetic field is

$$B_\theta=\frac{\mu_0 r}{2\pi R_d^2}I(z) \qquad [14]$$

B. *Tracking of Free Surfaces*

The moving free surface is tracked using a VOF function (F), which represents the VOF in the computational cell. The function F takes the value of 1 for the cell filled with the fluid and becomes 0 for the empty cell. If the cell is located on the free surface, the function F has a value between 0 and 1. The function F is governed by the equation[22]

$$\frac{\partial F}{\partial t}+\frac{1}{r}\frac{\partial}{\partial r}(ruF)+\frac{\partial}{\partial z}(wF)=0 \qquad [15]$$

C. *Boundary Conditions*

1. *Boundary conditions for momentum*

The boundary conditions needed to specify the fluid-flow problem are

(1) symmetry about the centerline,
(2) no slip at the solid boundaries,
(3) initially, the velocity of the electrode is taken as the wire feed rate, and
(4) at the free surface, the surface-tension pressure (P_s) can be expressed by[22]

$$P_s=\gamma\left(\frac{1}{R_1}+\frac{1}{R_2}\right) \qquad [16]$$

where γ is the surface-tension coefficient and R_1 and R_2 are the principal radii of the curvature of the surface. The Marangoni force due to the variation of the surface-tension coefficient with temperature (τ_s) is described by[8]

$$\tau_s = \mu \frac{\partial V_s}{\partial n} = \frac{d\gamma}{dT}\frac{\partial T}{\partial s} \quad [17]$$

The surface tension pressure and the Marangoni force are included by adding source terms to the momentum equation. The method used is detailed in Reference 23, which is called the continuum surface force model. For a planar surface, P_s is equal to zero and the surface-tension effects are only due to Marangoni force. For a curved surface, the two surface-tension effects act simultaneously.

2. *Boundary conditions for thermal energy*

The boundary conditions pertaining to the heat-transfer problem are

(1) symmetry about the axial centerline, and
(2) at the free surface of the molten pool, the heat flux from the welding arc is assumed to obey a Gaussian-type distribution of the form

$$-k\frac{\partial T}{\partial n} = \frac{\eta UI}{2\pi r_q^2}\exp\left(-\frac{r^2}{2r_q^2}\right) - h_c(T - T_\infty) \quad [18]$$

where h_c is a combined heat-transfer coefficient for the radiate and convective boundary expressed in the following equation:[24]

$$h_c = 24.1 \times 10^{-4}\,\varepsilon T^{1.61} \quad [19]$$

Dupont and Mander[25] indicated that the arc efficiency of the GMAW process is around 0.84, and that the superheated droplets account for 38 to 42 pct of the total power supplied to the workpiece. That is, the thermal energy to the weld pool provided by the welding arc is about 50 pct (0.84 · 0.6) of the total power input of the process. Thus, η is set as 0.5 in the calculation.

For the plasma-electrode interface, the heat flux from the arc plasma can be written as the sum of three contributions:[26,27]

$$k\frac{\partial T}{\partial n} = \frac{k_{\text{eff}}(T_{\text{arc}} - T_{\text{anode}})}{\delta} + j_a\phi_w + j_a\frac{5K_bT_e}{2e} \quad [20]$$

The first term on the right-hand side is the contribution due to thermal conduction from the plasma to the anode; the second term represents the electron heating associated with the work function of the anode material (ϕ_w); the last term accounts for thermal energy carried by the electrons into the anode. Here, T_{arc} is the arc temperature, which is assumed to have a constant value of 10^4 K at a distance (δ) of 0.1 mm away from the anode; T_{anode} is the anode temperature; k_{eff} is the effective thermal conductivity at the anode-plasma interface; and T_e is the electron temperature. It is stated in Reference 2 that, in the GMA welding of steel with a 1.2-mm-diameter electrode, the anodic area, or arc root, appears to cover the complete surface of the drop at a current of 140 A and at higher currents still covers the drop surface. Thus, j_a is approximated to be the square root of j_r^2 and j_z^2, which are calculated in Eqs [12] and [13].

The heat flux from the arc plasma (Eq. [20]) is considered to be a source term of the energy conservation equation in the cells along the plasma-electrode surface. The boundary conditions for the surfaces without heat input are expressed as

$$-k\frac{\partial T}{\partial n} = h_c(T - T_\infty) \quad [21]$$

3. *Electric-potential boundary conditions*

The boundary conditions concerning electrical potential in the area of the molten pool are as follows.

(1) There is symmetry about the centerline.
(2) An isopotential line ($\phi = 0$) is selected at the right wall because the right wall is far from the weld pool. A value of $\partial\phi/\partial z = 0$ is set at the bottom wall.
(3) At the free surface, the assumed Gaussian-type current flux is described by

$$-\sigma\frac{\partial\phi}{\partial n} = \frac{\mathrm{I}}{2\pi r_c^2}\exp\left(-\frac{r^2}{2r_c^2}\right) \quad [22]$$

IV. RESULTS AND DISCUSSION

A. *Impingement of the Droplet on the Substrate*

Figure 2 depicts the phenomena of droplet development and impingement of the droplet on the substrate. As shown in Figure 2(a), the mass of molten wire increases with time. For a current of 160 A, the pendant drop has a classic pear shape. Due to the competition among gravity, surface tension, electromagnetic force, and arc drag force, the droplet is elongated and a neck is formed before detachment. The current density in the droplet's neck increases because of the decrease of the current-carrying zone, which causes the electromagnetic force acting on the droplet to increase. As shown in Figure 2(b) (t = 204 ms), the velocity near the neck of the drop is much higher due to the sharp increase in the electromagnetic force. Thus, the electromagnetic force plays an important role in droplet detachment. Due to the combined effects of gravity, surface tension, and arc drag force, the detached droplet is accelerated in the arc plasma. The pear-shaped droplet becomes more spherical suggesting the influence of surface tension. Figure 2 shows a droplet formation time of approximately 204 ms, corresponding to a frequency of around 5 droplets per second. The calculated average diameter of the droplets is about 3.0 mm, which agrees well with the experimentally observed results shown in Figure 3.

After the droplet hits the substrate surface, it quickly spreads out on the substrate surface. As shown, the VOF flow in the molten pool rapidly decreases. An examination of the temperature contours in Figure 2(a) reveals that the substrate in the center region is more molten than that in the splat periphery due to its higher fluid temperature. This is because the splat periphery is continuously cooled by contact with the low-temperature surface of the substrate as it spreads outward. The heat input from the welding arc is another factor affecting the temperature distribution. As shown in Figure 3, the experimental results are in reasonable agreement with the predictions.

B. *The Last Droplet and Subsequent Solidification*

Around the time of 3 seconds, the arc is extinguished to observe the impact of the last droplet and subsequent

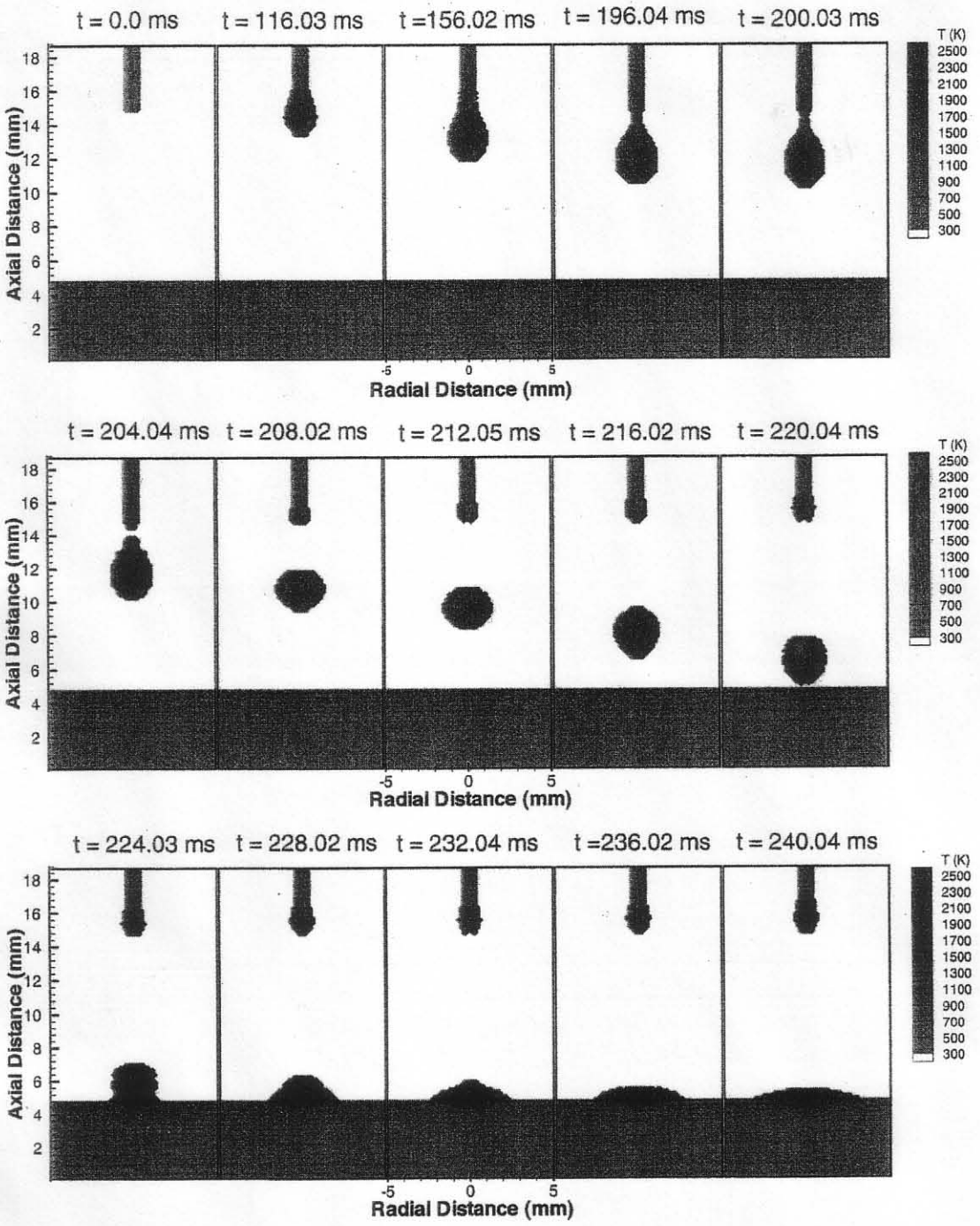

(*a*)

Fig. 2—(*a*) The temperature distribution in the process of the formation, impingement of the first droplet on the substrate. (*b*) The velocity distribution in the process of the formation, impingement of the first droplet on the substrate.

solidification. As the droplet impinges on the weld pool, there is a mixing of mass, momentum, and energy between the droplet and molten pool. The addition of the molten droplet increases the volume of the weld pool, the impact of the droplet causes a marked indentation in the weld pool, and the heat contained in the superheated droplet is transferred into the weld pool.

As shown in Figure 4, the model predicts that the falling droplet imparts kinetic energy to a region local to the surface, and this kinetic energy is expended in generating a cavity. At t = 3020 ms in Figure 4(b), the fluid is accelerated into the cavity, causing the cavity to fill immediately after impact (t = 3024 ms). An upward flow is induced at t = 3028 ms as a result of the impingement of inward flow at the center of the weld pool. Affected by inertia, a hump, which overpasses the equilibrium, is formed. That is, part of the kinetic energy has been transferred to potential energy. Under the influence of the hydrostatic, electromagnetic, and surface-tension forces,[28] the fluid moves downward at t = 3032 ms. Obviously, the downward flow will also pass the equilibrium of the aforementioned forces due to the inertia. Thus, it is seen that the fluid flow moves upward again at t = 3036 ms. Between the impingement of two consecutive drops, this

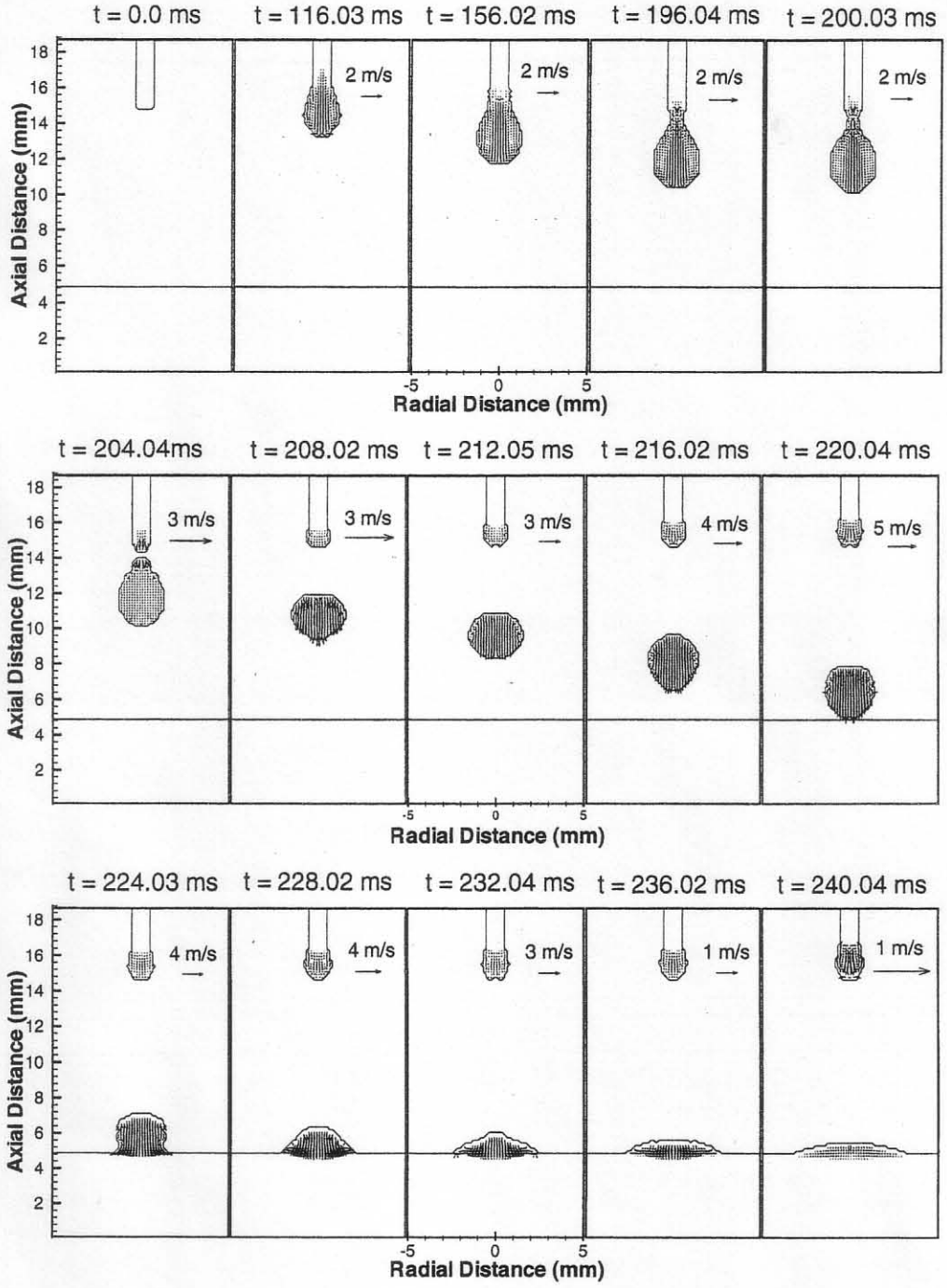

(*b*)

Fig. 2—(Continued) (*a*) The temperature distribution in the process of the formation, impingement of the first droplet on the substrate. (*b*) The velocity distribution in the process of the formation, impingement of the first droplet on the substrate.

loop will continue until equilibrium is achieved. This is called weld-pool oscillation.

The added high-temperature filler metal is driven downward by the stirring force due to the momentum of the falling droplets on the pool. Some experiments[29] have concluded that, in GMAW, the arc heat influences the depth of penetration only to a limited degree. As shown in Figure 4(a), the high-temperature filler metal could reach the bottom of the weld pool, which suggests that the penetration of the weld pool could be mainly determined by the impingement of droplets. After the arc extinguishes, the molten droplet and pool become smaller and smaller. Heat loss occurs mainly through the solid metal, so the liquid adjacent to the solid-liquid interface solidifies first. The last liquid zone is located in the tip of the droplet and on the top of the weld bead. The solidification of the droplet is completed after about 4 seconds, while solidification of the molten pool requires about 6 seconds. The size of the molten pool and the flow pattern are shown in Figure 4(b). The flow pattern in the weld pool describes the effect of convection on heat transfer and weld-pool oscillation clearly. It is also shown that the impingement of droplets is a key factor affecting the fluid

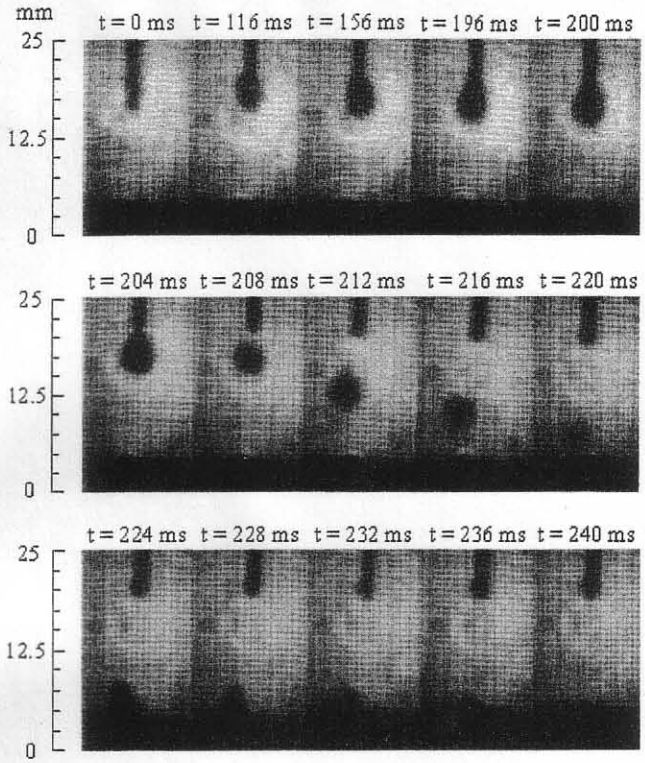

Fig. 3—Successive images of the formation, impingement of the first droplet on the substrate.

velocity. The fluid velocity increases significantly after impingement and decreases gradually in the process of solidification.

The experimental images are shown in Figure 5. Although the cavity in the center of the weld pool could not be observed under the current experimental conditions, the obtained images show that the weld-pool oscillation could be triggered by the impingement of a droplet and that the amplitude of the oscillation decreases gradually.

The resultant weld bead is shown in Figure 6. The actual penetration is less than the predicted results in Figure 4(b), and the penetration is not finger-like. In the modeling, we assume that the droplets always impact the center of the molten pool. In actual stationary GMAW, the droplets never hit the molten pool at the same place every time, thus resulting in a shallower penetration. They do not hit the same place every time because the droplet formation and detachment and the droplet transfer in arc plasma are affected by several factors which cannot be defined strictly, and when the droplets hit the weld pool they cause movement of that pool. Thus, the subsequent drop hits a slightly different spot in the pool and, therefore, cannot penetrate as deeply. In addition, the periodically injected droplets result in a high-reinforcement bead profile in stationary gas metal arc welding. Since it is difficult for falling droplets to reach the bottom of the weld pool because of the bead height, the heat cannot be transferred to the weld root efficiently. As a result, there is no finger-shaped penetration. For welding, the increase of the droplet transfer rate could cause the well-known finger-shaped penetration. With the increase of the droplet transfer rate, the droplets are more easily directed to one point. The cavity caused by the impingement of the droplets could not be filled in time because of the higher droplet transfer rate. The droplets fall constantly in the same cavity, so that the heat is transferred efficiently to the weld root.

Since the weld-surface profile is controlled by surface tension, and the locations of impact of the drops on the workpiece are not a dominant factor, the predicated surface profile agrees well with the resultant weld bead.

V. CONCLUSIONS

The globular transfer in stationary GMAW, including droplet formation, detachment, and impingement on the molten pool, has been dynamically simulated using a modified SOLA-VOF method. The principal conclusions are summarized as follows.

In the process of droplet formation, the size and the transfer frequency of the large droplets of globular transfer are determined by the balance of gravity, surface tension, electromagnetic force, and arc drag force. The electromagnetic force is a key factor affecting droplet detachment. The detached droplet is accelerated and rounded in the arc plasma.

The weld-pool oscillation could be triggered by the impingement of the droplets. The frequency and amplitude of pool oscillation are closely connected to the momentum of the droplets.

It is suggested that the droplet transfer frequency has a major influence on the weld-pool configuration. A higher frequency leads to a deeper penetration. The locations where the droplets impinge on the weld pool are another important factor that affects pool shape. The scattere dimpinging locations could result in a shallower and wider weld shape instead of the normal finger shape.

The calculated temperature distribution reveals that the fluid temperature around the periphery is lower than the temperature at the center. Solidification, therefore, is expected to initiate at the solid-liquid interface and advance toward the center. It is noticed that the velocity of falling droplets is an important factor in determining the velocity field in the molten pool.

A high-speed video camera has been used to record the images of the metal transfer process. The calculated results agree well with the experimental results.

ACKNOWLEDGMENTS

This work was supported by the National Science Foundation under Grant No. DMI-9732848 and THECB/ATP Grant No. 003613-005, which is gratefully acknowledged. The authors also appreciate the assistance of Dr. B. Zheng, I. Kmecko, and M. Labudovic in the experimental work.

NOMENCLATURE

B_θ	azimuthal magnetic field
C_p	heat capacity
D_d	droplet diameter
f	droplet transfer frequency
f_L	liquid fraction
F	volume of fluid
g	gravitational acceleration
h	specific enthalpy

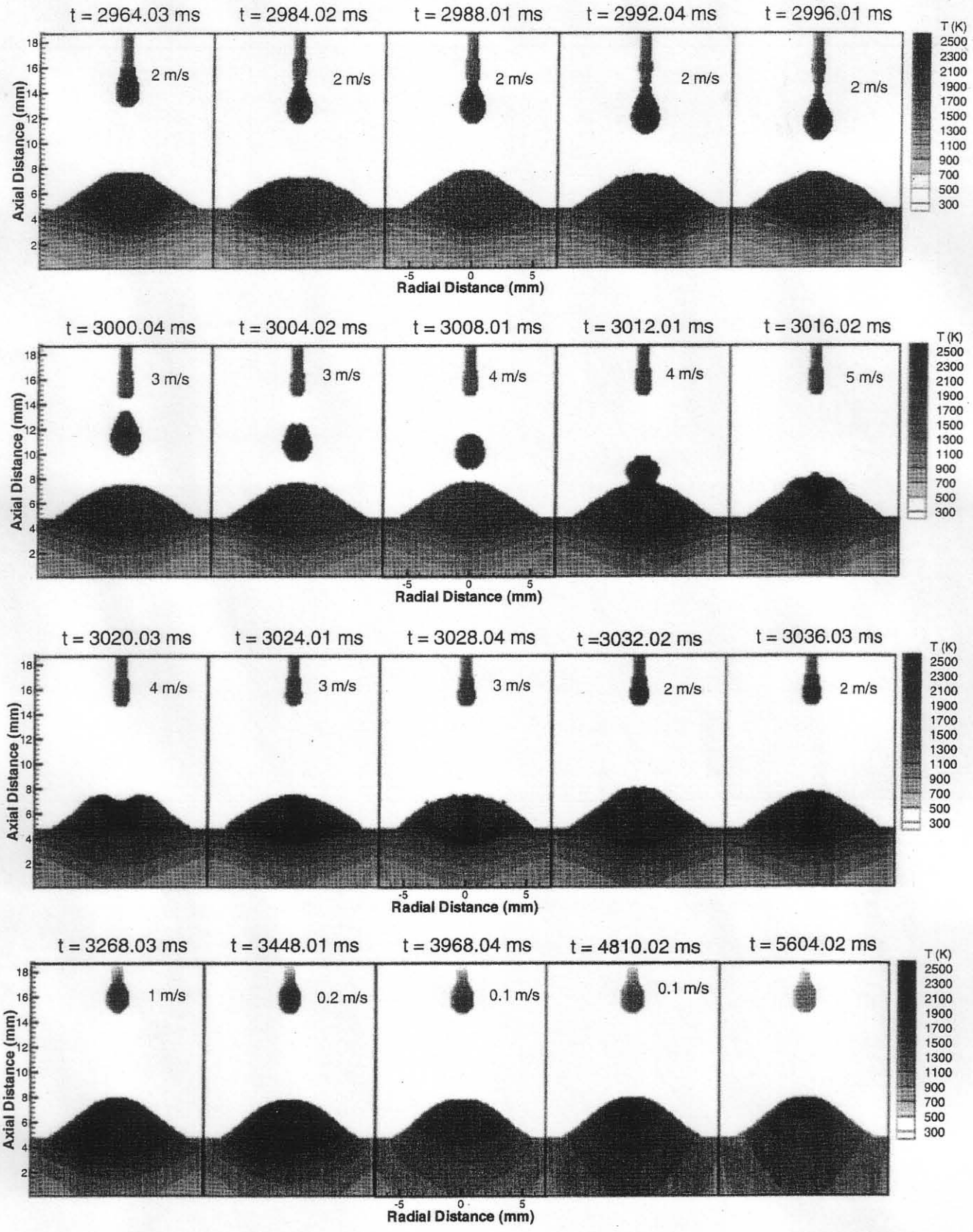

(*a*)

Fig. 4—(*a*) The temperature distribution in the process of the formation, impingement of the last droplet and subsequent solidification. (*b*) The velocity distribution in the process of the formation, impingement of the last droplet and subsequent solidification.

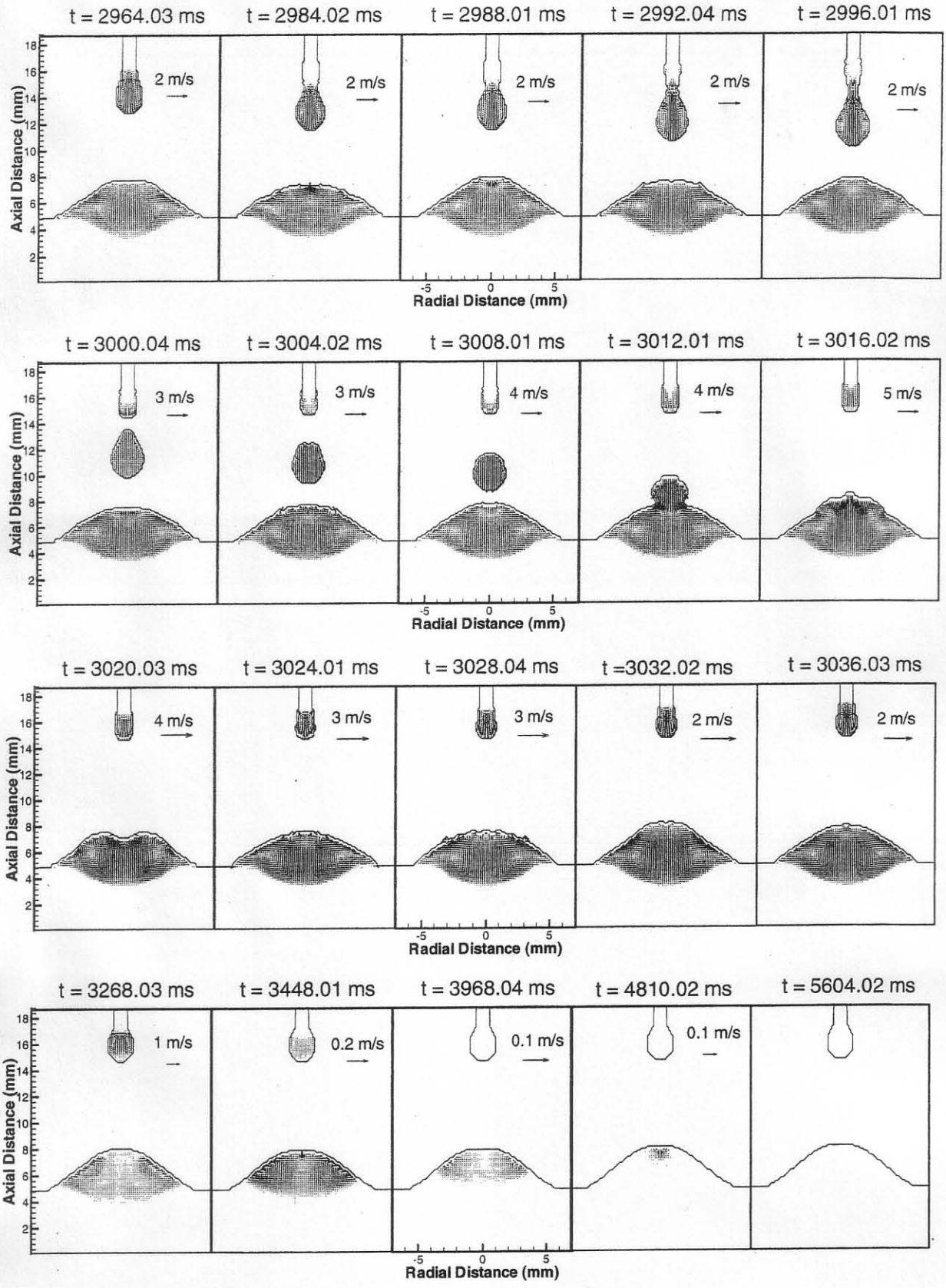

(*b*)

Fig. 4—(Continued) (*a*) The temperature distribution in the process of the formation, impingement of the last droplet and subsequent solidification. (*b*) The velocity distribution in the process of the formation, impingement of the last droplet and subsequent solidification.

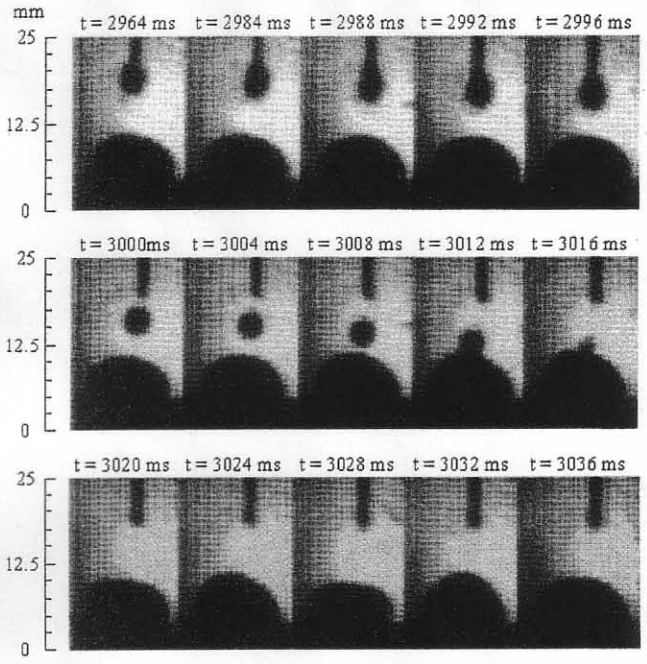

Fig. 5—The images for the formation, impingement of the last droplet on the molten pool.

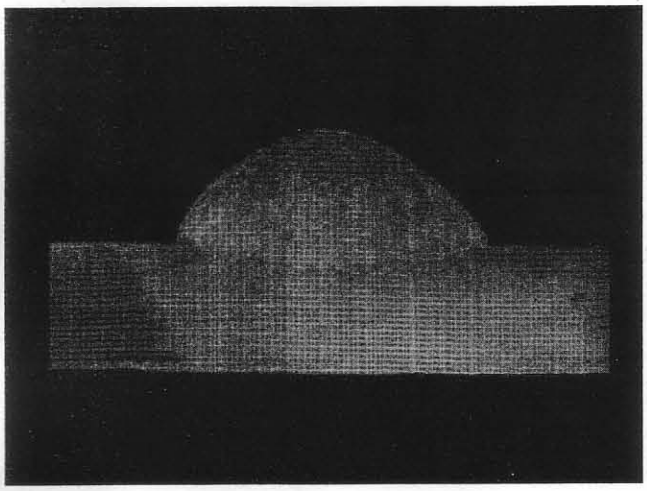

Fig. 6—The cross section of the resultant weld bead.

h_c	combined heat-transfer coefficient at the surface
I	arc current
j_a	current density at the anode
j_r, j_z	radial, axial current density
k	thermal conductivity
k_{eff}	effective thermal conductivity
K	drag index in source term
K_b	Boltzmann's constant
$K_{\max}$	maximum drag index
n	normal direction to surface
P	pressure
r_q, r_c	heat, current flux distribution radius
r, z	radial, axial coordinate
R_d	radius of the droplet
s	tangential direction along surface
S	source term
t	time
T	temperature
T_{anode}	anode temperature
T_{arc}	arc temperature
T_e	electron temperature
T_r	reference temperature
T_∞	surrounding temperature
T_l	liquidus temperature
T_m	melting temperature
T_s	solidus temperature
u, w	radial, axial velocity
U	arc voltage
V_{arc}	velocity of arc plasma
V_n	normal velocity component at molten pool surface
V_s	tangential velocity component at molten pool surface
V_w	wire feed speed
ΔH	latent heat of fusion

Greek Symbols

β	coefficient of thermal expansion
η	arc efficiency
μ	viscosity
μ_0	permitivity of free space
ρ	density
ρ_{arc}	density of arc plasma
σ	electrical conductivity
ϕ	potential
γ	surface tension
$d\gamma/dT$	temperature gradient of surface tension
ε	emissivity of body surface

REFERENCES

1. J.H. Waszink and L.H.J. Graat: *Weld. J.*, 1983, vol. 62, pp. 109s-116s.
2. J.F. Lancaster: *The Physics of Welding*, Pergamon, Oxford, United Kingdom, 1986.
3. C.J. Allum: *J. Phys. D: Appl. Phys.*, 1985, vol. 18, pp. 1431-46.
4. C.J. Allum: *J. Phys. D: Appl. Phys.*, 1985, vol. 18, pp. 1447-68.
5. V.A. Nemchinsky: *J. Phys. D: Appl. Phys.*, 1994, vol. 27, pp. 1433-42.
6. S.W. Simpson and P.Y. Zhu: *J. Phys. D: Appl. Phys.*, 1995, vol. 28, pp. 1594-1600.
7. J. Haidar and J.J. Lowke: *J. Phys. D: Appl. Phys.*, 1996, vol. 29, pp. 2951-60.
8. J. Haidar: *J. Appl. Phys.*, 1998, vol. 84, pp. 3518-40.
9. A. Lesnewich: *Weld. J.*, 1958, vol. 37, pp. 343s-353s and 418s-42s.
10. Y.S. Kim and T.W. Eagar: *Weld. J.*, 1993, vol. 72, pp. 269s-278s.
11. S. Rnee and E. Kannatey-ashibu, Jr.: *Weld. J.*, 1992, vol. 72, pp. 381s-386s.
12. L.A. Jones, T.W. Eagar, and J.H. Lang: *Weld. J.*, 1998, vol. 77, pp. 135s-141s.
13. Y.H. Xiao and G. den-Ouden: *Weld. J.*, 1990, vol. 69, pp. 289s-293s.
14. Y.H. Xiao and G. den-Ouden: *Weld. J.*, 1993, vol. 72, pp. 428s-434s.
15. K. Andersen, G.E. Cook, and R.J. Barnett: *IEEE Trans. Ind. Appl.*, 1997, vol. 33, pp. 464-71.
16. A.J.R. Aendenroomer and G. den-Ouden: *Weld. J.*, 1998, vol. 77, pp. 181s-187s.
17. K.C. Tsao and C.S. Wu: *Weld. J.*, 1988, vol. 67, pp. 70s-75s.
18. J.W. Kim and S.J. Na: *Trans. ASME*, 1994, vol. 116, pp. 78-85.
19. M. Ushio and C.S. Wu: *Metall. Mater. Trans. B*, 1997, vol. 28B, pp. 509-17.
20. S.K. Choi, S.H. Ko, C.D. Yoo, and Y.S. Kim: *Weld. J.*, 1998, vol. 77, pp. 45s-51s.
21. G. Trapaga: *Metall. Trans. B*, 1992, vol. 23B, pp. 701-18.
22. B.D. Nichols, C.W. Hirt, and R.S. Hotchkiss: "SOLA-VOF: A Solution Algorithm for Transient Fluid Flow with Multiple Free Boundaries," Report No. LA-8355, Los Alamos Scientific Laboratory, Los Alamos, NM, 1980.
23. D.B. Kothe, R.C. Mjolsness, and M.D. Torrey: "RIPPLE: A Computer

Program for Incompressible Flows with Free Surfaces," Report No. LA-12007-MS, Los Alamos Scientific Laboratory, Los Alamos, NM, 1991.
24. J. Goldak, M. Bibby, J. Moore, and B. Patel: *Metall. Trans. B*, 1986, vol. 17B, pp. 587-600.
25. J.N. Dupont and A.R. Marder: *Weld. J.*, 1995, vol. 74, pp. 406s-416s.
26. P.Y. Zhu, M. Rados, and S.W. Simpson: *Weld. J.*, 1997, vol. 76, pp. 269s-274s.
27. P.G. Jonsson, T.W. Eagar, and J. Szekely: *Metall. Mater. Trans. B*, 1995, vol. 26B, pp. 383-98.
28. V.A. Nemchinsky: *J. Phys. D: Appl. Phys.*, 1996, vol. 29, pp. 2659-63.
29. W.G. Essers and R. Walter: *Weld. J.*, 1981, vol. 61, pp. 37s-58s.